ADVANCED FUNCTIONAL MATERIALS
www.afm-journal.de

Molybdenum Dioxide in Carbon Nanoreactors as a Catalytic Nanosponge for the Efficient Desulfurization of Liquid Fuels

*Maxwell A. Astle, Graham A. Rance, Hannah J. Loughlin, Thomas D. Peters, and Andrei N. Khlobystov**

The principle of a "catalytic nanosponge" that combines the catalysis of organosulfur oxidation and sequestration of the products from reaction mixtures is demonstrated. Group VI metal oxide nanoparticles (CrO_x, MoO_x, WO_x) are embedded within hollow graphitized carbon nanofibers (GNFs), which act as nanoscale reaction vessels for oxidation reactions used in the decontamination of fuel. When immersed in a model liquid alkane fuel contaminated with organosulfur compounds (benzothiophene, dibenzothiophene, dimethyldibenzothiophene), it is found that MoO_2@GNF nanoreactors, comprising 30 nm molybdenum dioxide nanoparticles grown within the channel of GNFs, show superior abilities toward oxidative desulfurization (ODS), affording over 98% sulfur removal at only 5.9 mol% catalyst loading. The role of the carbon nanoreactor in MoO_2@GNF is to enhance the activity and stability of catalytic centers over at least 5 cycles. Surprisingly, the nanotube cavity can selectively absorb and remove the ODS products (sulfoxides and sulfones) from several model fuel systems. This effect is related to an adsorptive desulfurization (ADS) mechanism, which in combination with ODS within the same material, yields a "catalytic nanosponge" MoO_2@GNF. This innovative ODS and ADS synergistic functionality negates the need for a solvent extraction step in fuel desulfurization and produces ultralow sulfur fuel.

1. Introduction

Despite the advancement of environment-friendly technologies, the transportation and energy industries still depend heavily on diesel fuel. However, recent trends of increased diesel consumption and the dwindling reserves of crude oil have triggered questions about satisfying the demand for the future.[1,2] Moreover, the available sources of crude oil contain a high content of refractory sulfur compounds, which can have adverse industrial and environmental effects, including the formation of acid rain.[3,4] Therefore, a key current research challenge concerns the development of an efficient and economically viable process to remove sulfur-containing contaminants from fuels in order to satisfy the ultralow sulfur diesel (ULSD) regulations of less than 10 ppm imposed by international policies.[5–7]

For industrial applications, the removal of sulfur compounds by hydrodesulfurization (HDS) is currently the most widely utilized process; yet, it has several disadvantages, including harsh reaction conditions, high costs, and limited applicability to the aromatic sulfur compounds.[8] As a result, the development of other desulfurization processes has been more recently explored (**Figure 1**). With biodesulfurization (BDS) currently hindered by low enzyme activity and stability, oxidative desulfurization (ODS), and adsorptive desulfurization (ADS) technologies offer more realistic promise.[9–11] Specifically, the use of ODS to remove the refractory sulfur compounds from fuels exploits key changes in the polarity of the oxidized products relative to the parent organosulfur contaminant during extraction and has already been established for the production of ULSD.[12] However, limiting the quantity of solvent needed to avoid fuel loss during extraction and the lack of cheap, efficient, and readily recoverable catalysts represent major stumbling blocks for this pathway.[6] ADS has also shown reasonable success, utilizing the physical adsorption of organosulfur compounds within the internal volumes of porous materials, such as zeolites, aluminosilicates, and activated carbon.[13–15] However, a new strategy for active materials with high and specific adsorption capacity for sulfur compounds is needed urgently. Therefore, significant further research is required to improve these individual strategies for ULSD production, which could be based on more than one desulfurization mechanism simultaneously, as we demonstrate in this study.

M. A. Astle, Dr. G. A. Rance, H. J. Loughlin, T. D. Peters, Prof. A. N. Khlobystov
School of Chemistry
University of Nottingham
University Park
Nottingham
NG7 2RD, UK
E-mail: Andrei.Khlobystov@nottingham.ac.uk
Dr. G. A. Rance, Prof. A. N. Khlobystov
Nanoscale and Microscale Research Centre
University of Nottingham
University Park
Nottingham
NG7 2RD, UK
The ORCID identification number(s) for the author(s) of this article can be found under https://doi.org/10.1002/adfm.201808092.

DOI: 10.1002/adfm.201808092

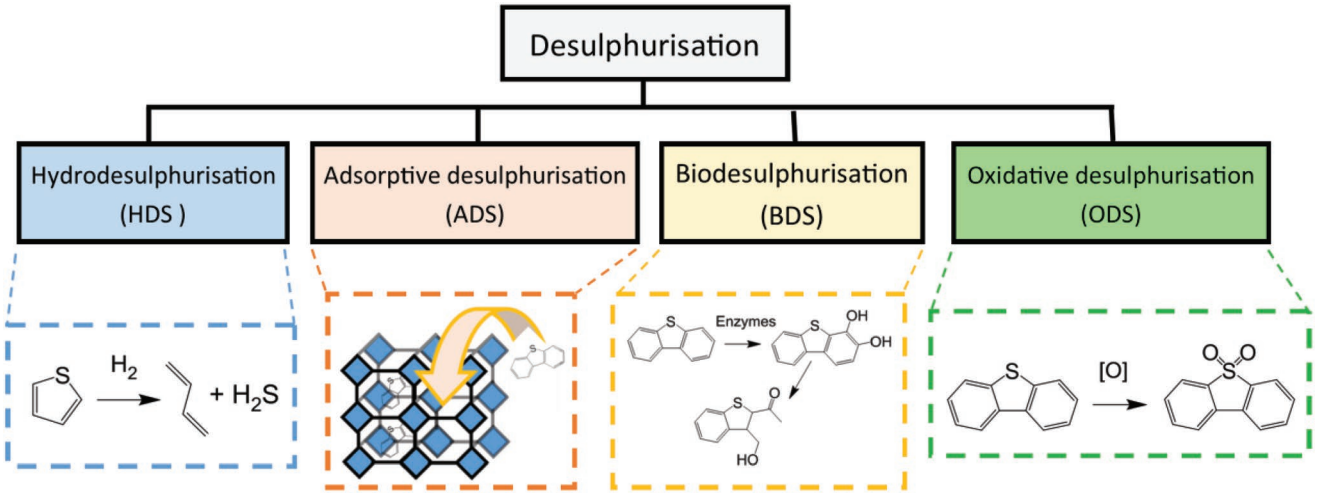

Figure 1. Current strategies for the desulfurization of fuel. The application of hydrodesulfurization (HDS) for aromatic sulfur compounds, such as thiophene uses hydrogen and produces H_2S. Adsorptive desulfurization (ADS) using porous media and biodesulfurization (BDS) via the Kodama pathway in the presence of enzymes have both shown promise for the selective removal of dibenzothiophene (DBT). Oxidative desulfurization (ODS) has the greatest potential for oxidation of DBT, yielding ultralow sulfur fuels.

We selected molybdenum oxide because it has recently emerged as a promising material for the ODS of fuel,[16–18] with the ease of formation of the electrophilic molybdenum peroxo intermediate species identified as the driving force for the effective oxidation of the sulfur contaminants (**Figure 2**).[19] This intermediate is produced when an oxidant, such as hydrogen peroxide, reacts with the Lewis acidic sites of the metal oxide and leads to the formation of electrophilic species, essential to promote efficient ODS. In addition, the performance of molybdenum-based nanocatalysts can be optimized using support materials, which are known to both stabilize nanoparticles against sintering and promote further activity by facilitating charge transfer between the catalysts and the support material. Al_2O_3, TiO_2, and SiO_2 supports have recently been shown to improve the performance of ODS catalysts, therefore, selection of an appropriate support is key for refining the oxidative removal of sulfur contaminants in fuel.[20–23] Among catalyst supports, hollow carbon nanostructures, such as carbon nanotubes, may offer several potential benefits for ODS catalysts.[24,25] Hollow graphitized nanofibers (GNFs) with an internal diameter of 60 nm—structural analogues to carbon nanotubes, but possessing nanoscale step-edges on the inside—are particularly attractive as their corrugated interior surfaces promote the formation and enhance the stability of catalytic centers,[26–28] while increasing the concentration of reactants around the catalyst, without restricting the transport of reactants to and products from the internal cavity (the critical dimensions of most small molecules are typically at least two orders of magnitude smaller than the internal diameter of GNFs).[29,30] Furthermore, as porous activated carbons have shown promise in the desulfurization of fuels via ADS,[31,32] we anticipated that GNFs, possessing the high internal surface area of nanotubes and maximal π–π stacking interactions between guest and host at the graphitic step-edges, may offer enhanced extraction of aromatic organosulfur contaminants, promoting simultaneous desulfurization via both the ADS and ODS mechanisms.[33]

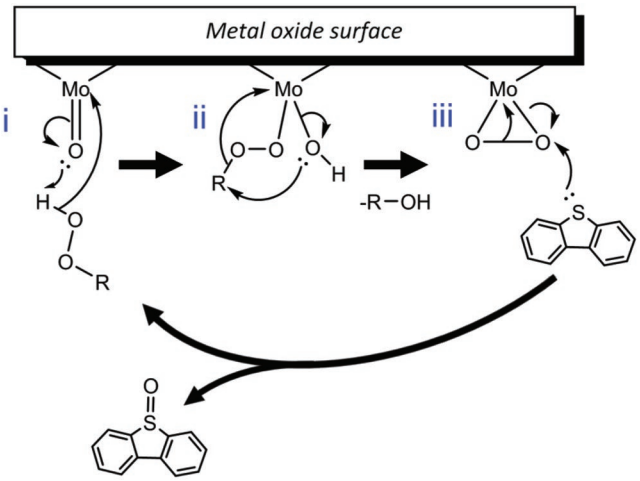

Figure 2. Mechanism for the oxidation of sulfur contaminants using molybdenum oxide catalysts with peroxide species. (i) Nucleophilic attack of the peroxide forms the hydroperoxymolybdate species. (ii) Reversible loss of alcohol to produce the monoperoxo species. (iii) The peroxo group is activated electrophilically via coordination to the molybdenum atoms and results in a nucleophilic attack from the sulfur atom in the organosulfur species and loss of the oxidized product.

In this work, chromium, tungsten, and molybdenum oxide nanoparticles were grown within GNF cavities to form carbon nanoreactors, with the latter extensively applied to the ODS of liquid fuels. The catalytic nanoreactor MoO_2@GNF demonstrated the best activity for ODS and revealed a surprising nanosponge effect by absorbing and sequestering the oxidized contaminants from liquid alkane fuel by ADS. The combined ADS and ODS activities within the same material lead to ultralow sulfur fuels without solvent extraction, thus making a significant advancement toward the production of ULSD.

2. Results and Discussion

2.1. Synthesis and Characterization of Molybdenum Dioxide Nanoparticles Encapsulated within Hollow Graphitized Carbon Nanofibers

The filling of hollow GNFs can be readily achieved by exposing empty GNFs to suitable precursors that contain the desired elements, sublime readily at relatively low temperatures, are stable in the gas-phase and decompose into the desired species using external stimuli.[34] Molybdenum dioxide bisacetylacetonate ($MoO_2(acac)_2$) was thus identified as an ideal precursor and adopted for the gas-phase thermal deposition reaction. Sealing GNFs and the precursor under vacuum (3×10^{-5} mbar) allows the sublimed guest-molecules to diffuse into the empty nanofibers (**Scheme 1**); once trapped within the nanofiber cavity, the precursor molecules are heated in an inert atmosphere to facilitate decomposition into molybdenum oxide nanoparticles entrapped in GNFs (MoO_x@GNF).

To confirm the oxidation state and crystallinity of the molybdenum oxide species within the composite material powder X-ray diffraction (PXRD) analysis was employed. Peaks at $2\theta = 37.1°$ and 53.6° can be clearly observed in the diffractogram, consistent with the crystal phase of molybdenum(IV) dioxide (**Figure 3**a).[35] Thermogravimetric analysis (TGA) showed the loading (by weight) of the metal oxides in the final composite as 4.0% (Figure 3b). In addition, TGA also indicates a significant reduction in the combustion temperature of the GNF by more than 150 °C, indicating intimate contact between the nanoparticles and the nanofibers, which are important for the catalytic performance in ODS.[28] Energy dispersive X-ray (EDX) spectroscopy reveals the elemental composition of the MoO_2@GNF, with a near 2:1 atomic ratio of oxygen to molybdenum, further supporting the formation of the dioxide species (Figure 3c).

To evaluate the size, morphology, and position of the molybdenum dioxide nanoparticles within GNFs, transmission electron microscopy (TEM) is essential. Statistical analysis of images taken from multiple parts of the specimen grid indicates nanoparticles with an average diameter of 29 ± 10 nm are found predominantly within the internal cavity of the GNFs, with their distinctive contrast relative to the carbon of the GNF strongly supporting the formation of metal oxide (**Figure 4**b). Thus, this technique offers superior control over the size and location of metal oxide nanoparticles inside hollow carbon nanofibers relative to previously reported electrospinning approaches.[36] The interior surfaces appear to be the favored site for the growth of nanoparticles relative to the external walls, confirming the importance of step-edges which provide anchoring points for nucleation of the metal oxide, which are absent on the smooth graphitic layers of the exterior. High-resolution TEM of the nanoparticles reveals a *d*-spacing of 0.37 nm, which corresponds to the set of (110) lattice planes of MoO_2 (Figure 4c). Scanning transmission electron microscopy (STEM) in combination with EDX elemental mapping additionally confirms the composition of the nanoparticles as molybdenum and oxygen (Figure S1, Supporting Information). To extract information on the 3D structure of the nanoparticles, images were captured at different extents of angular tilt (Figure 4d). As the GNF is rotated around its growth axis it can be observed that the MoO_2 nanoparticles remain within the interior channel confirming their confinement within the internal volume without hindering transport resistance and exhibit faceted morphologies.

To probe the ability to control the structure and composition of the metal oxide nanoparticles by postsynthesis treatments, small quantities of the sample were heated to elevated temperatures in air (**Figure 5**a). The previous TGA measurements (Figure 2b) indicate that thermal treatment at 270 °C results in a transformation from MoO_2 to MoO_3; this transition was additionally observed in the in situ PXRD, with peaks at $2\theta = 27.4°$, 33.9°, and 39.3° observed above 250 °C consistent with the formation of MoO_3. In addition, the thermal treatment resulted in an increase of the MoO_3 particle size to 63 ± 22 nm (Figure 5c). Therefore, this strategy offers an effective mechanism for controlling both the size and the composition of the metal oxide nanoparticles. Moreover, the large number of possible group VI precursors that readily sublime at low to moderate temperatures opens the door for a broad range of different catalytic nanoreactors that can be readily afforded and manipulated using this simple and versatile strategy (Figure 5d,e).

2.2. Catalytic Performance of MoO_2@GNF towards Oxidative Desulfurization of Fuel

To appraise the hybrid material for its ability to desulfurize fuel, a model system comprising 500 ppm dibenzothiophene (DBT) in *n*-hexane was identified.[37,38] DBT was selected as it is commonly found in oil, thus presenting a real and important environmental issue in its own right, and has distinctive absorption features in the UV–vis spectrum, ensuring facile measurement of its concentration in model fuels (Figure S2, Supporting Information). The aliphatic hydrocarbon *n*-hexane is a common

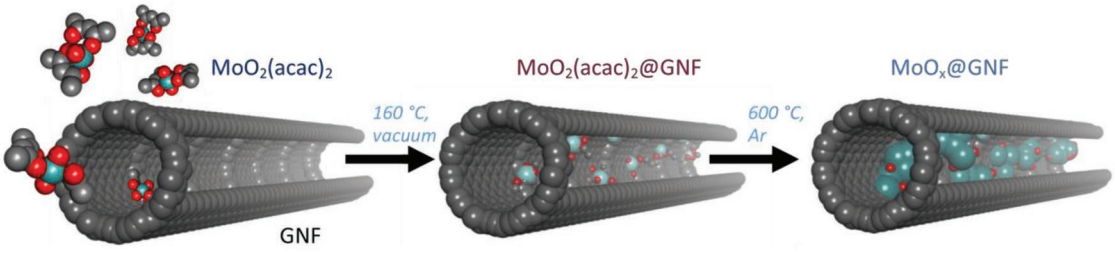

Scheme 1. Schematic diagram for the gas-phase encapsulation of $MoO_2(acac)_2$ and thermal growth of molybdenum oxide nanoparticles encapsulated within the hollow graphitized carbon nanofibers.

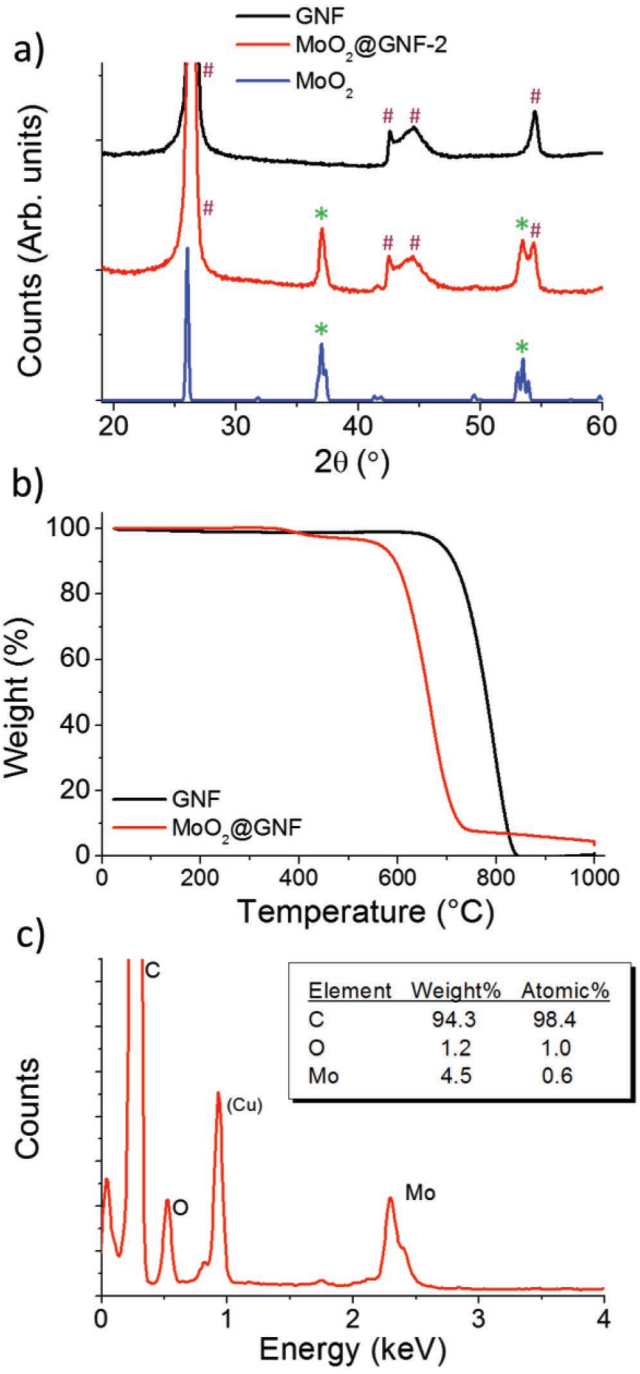

Figure 3. a) PXRD patterns of MoO_2@GNF (red), empty GNF (black), and bulk MoO_2 (blue) show that the hybrid material is the combination of the two components. Grain size was estimated to be 20 nm based on analysis of the peak at $2\theta = 37.1°$ (full width half maximum = 0.51°) and application of the Scherrer equation. b) Representative TGA of MoO_2@GNF (red) versus GNF (black), providing a measure of the metal oxide loading. c) EDX spectroscopy of MoO_2@GNF confirms the presence of Mo and O inside GNF in a ratio close to the stoichiometry in MoO_2.

constituent of fuel and represents a valuable model fuel simulant used in previous research.[39]

In a typical ODS procedure, an organic peroxide—employed to avoid potential phase transfer limitations—in a ratio of 1:20 (S:O) was added to the model fuel and catalyst and stirred at 60 °C for 120 min.[6,21,37,39] Consistent with previous studies, we subsequently employed an extraction procedure in which the model fuel was vigorously stirred with acetonitrile (in a 1 to 5 ratio of extractant to fuel) for 30 min.[21,38] Acetonitrile was selected as the solvent due to its known effectiveness toward the extraction of the DBT oxidation products and its reduced toxicity relative to other commonly utilized extraction solvents, such as dimethylformamide.[40] Interestingly, it was noted that 27–30% of DBT can be removed from the fuel simply through extraction alone, reflecting the moderate solubility of DBT in *n*-hexane. This was confirmed by treating the model fuel with the combined ODS and extraction procedure with either no catalyst or empty GNFs (**Table 1**, entries 1–2), both of which resulted in no DBT oxidation, but yielded DBT removal of 28.8% and 28.6% from the model fuel, respectively. These control tests clearly demonstrate that neither the extraction solvent nor empty GNFs are able to desulfurize model fuel to satisfactory levels.

A 5 mg quantity of MoO_2@GNF catalyst (containing 4 wt% MoO_2) was then added to the model fuel to assess its ability to remove the contaminants by ODS. Remarkably, after 120 min of the ODS reaction and subsequent solvent extraction 98.8% removal of the DBT from the model fuel was achieved (Table 1, entry 3 and **Figure 6**a). Experiments conducted using shorter reaction times, but with variable quantities of catalyst, indicated that in principle even more effective sulfur removal could be realized by increasing the loading of MoO_2@GNF present in the reaction mixture (Table S1, Supporting Information). ^{1}H nuclear magnetic resonance (NMR) spectroscopy and gas chromatography–mass spectrometry (GC-MS) of the combined sulfur contaminants in the solvent extraction phase and the washed solid catalyst confirms the high efficiency of DBT oxidation (96.8% conversion) leading predominantly to the doubly oxidized sulfone product (Figure S3, Supporting Information). The driving force for effective oxidation of the sulfur contaminants using our catalytic nanoreactors strongly relates to the environment at which the catalyst resides, with both modulated surface reactivity and heightened local concentrations of the contaminant at the GNF step-edge where the catalyst is located, as previously demonstrated for reactions of hydrosilylation.[27]

To further explore the importance of step-edges, a sample of MoO_2 on graphite was produced (Figure S4, Supporting Information). Graphite flakes provide anchoring sites for the catalyst, akin to GNFs, but no confinement as inside the GNFs. The results of catalyst performance showed that DBT oxidation still occurred, yet to a lesser extent than observed using MoO_2@GNF, with a reduction of 27% in organosulfur removal noted (Table 1, entry 5). This supports the notion that confinement of catalysts within GNF nanoreactors is important, here affording smaller, more active, nanoparticles (Figure S5, Supporting Information) and higher local concentrations of DBT molecules at the GNF internal step-edges relative to the smoother surfaces of graphite, both of which enhance ODS activity. Moreover, TEM indicates that after the ODS reaction MoO_2 nanoparticles remain practically unchanged inside GNFs, thus the interior of GNF provides the ideal protective environment, inhibiting nanoparticle desorption and leaching, ensuring the reuse of the catalyst in subsequent ODS reactions (Figure S6, Supporting Information).

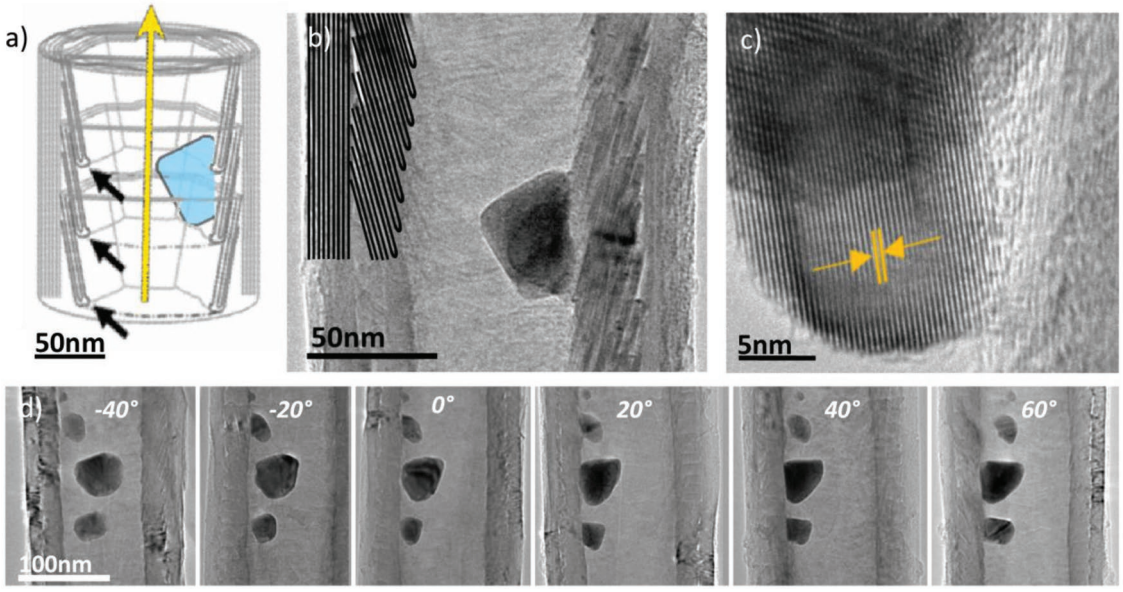

Figure 4. a) Schematic representation of the structure of GNFs (interior step-edges are denoted by black arrows; the yellow arrow signifies the direction of the nanofiber growth axis; the blue shape represents a MoO_2 nanoparticle). b) Bright field transmission electron microscopy image MoO_2@GNF. The internal step edges have been highlighted for clarity, with the MoO_2 nanoparticle clearly shown residing at the interior step-edges. c) High-resolution TEM of the MoO_2 nanoparticle providing a lattice spacing of 0.37 nm, consistent with the (100) plane in MoO_2. d) TEM tilt series of MoO_2@GNF, rotating around the GNF growth axis, which allows for a better understanding of the morphology of the nanoparticles and confirms their encapsulation within the internal cavity of the GNF.

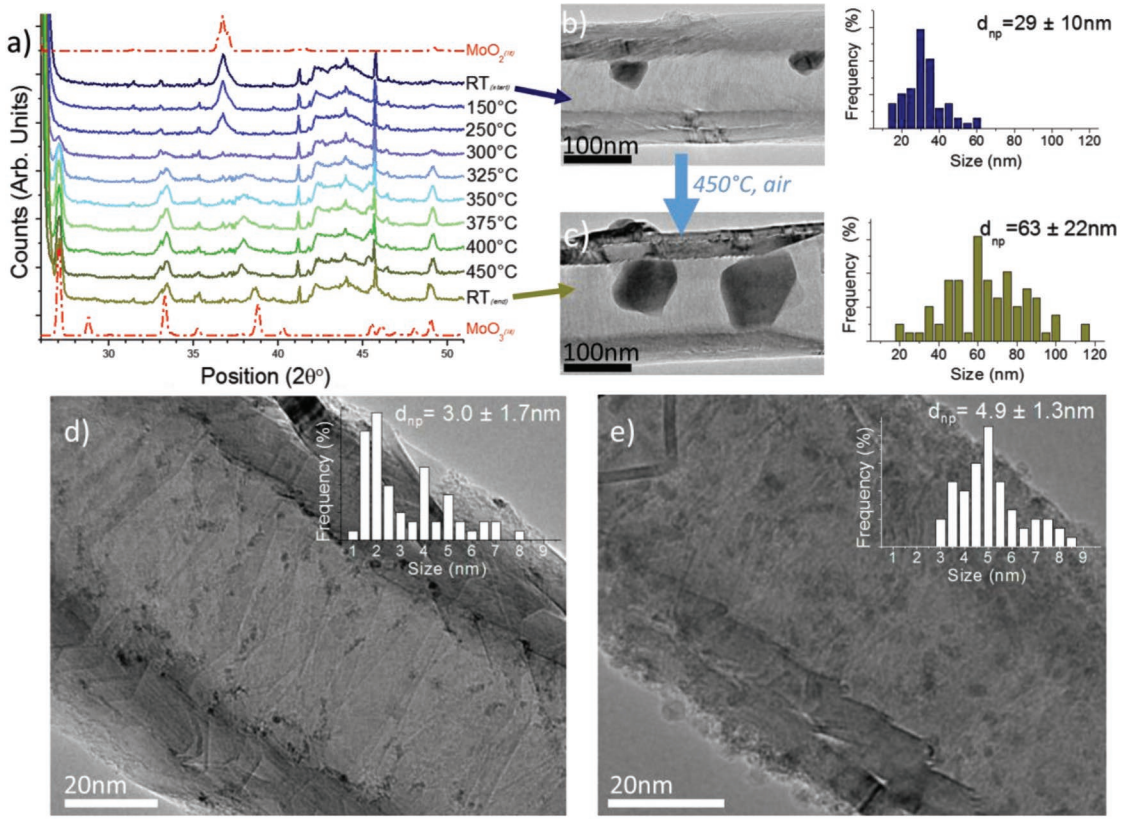

Figure 5. a) PXRD analysis of MoO_2@GNF thermally annealed in air clearly shows the change from MoO_2 to MoO_3 between 250 and 300 °C. b,c) TEM images and corresponding nanoparticle size distributions before and after postsynthesis thermal treatment at 450 °C, respectively, highlighting the increase in nanoparticle size and blocking of the GNF interior channel for materials treated at elevated temperatures. d,e) TEM images of WO_x@GNF (from $W(CO)_6$) and CrO_x@GNF (from $Cr(acac)_3$) with their particle size distribution profiles, respectively. These show the potential of the gas-phase deposition technique using different precursors to produce a plethora of unique nanomaterials.

Table 1. Dibenzothiophene removal from the model fuel system.

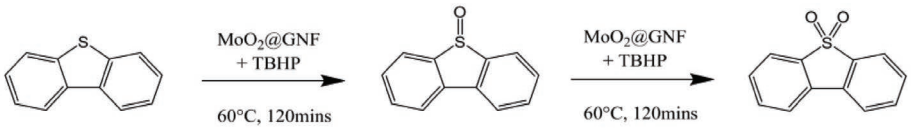

Dibenzothiophene (DBT) → *Dibenzothiophene sulfoxide (DBTO)* → *Dibenzothiophene sulfone ($DBTO_2$)*

Entry	Catalyst[a)]	Sulfur removal with ODS procedure only[b)] [%]	Sulfur removal with ODS and solvent extraction[b)] [%]	DBT conversion[c)] [%]	Selectivity[c)] [%] DBTO:$DBTO_2$	Turnover frequency[d)] [mol mol^{-1} min^{-1}]
1	None	0.0	28.8 (29.4)	0.0	-: -	–
2	GNF	0.0	28.6 (30.1)	0.0	-: -	–
3	MoO_2@GNF	95.5	98.8 (98.1)	96.8	14:86	0.14 (0.45)
4	MoO_3@GNF	46.3	72.7 (75.1)	57.2	76:24	0.08
5	MoO_2@graphite	44.4	71.5 (74.2)	60.8	75:25	0.09

[a)]5 mg catalyst (containing 4 wt% MoO_x), 5 mL of *n*-hexane containing 500 ppm DBT, tert-butyl hydroperoxide (TBHP) oxidant (S:O is 1:20), 60 °C, 120 min; [b)]Percentage of sulfur-containing contaminants removed via either (i) ODS or (ii) combined ODS solvent extraction (1 mL CD_3CN, 30 min) was determined using UV–vis spectroscopy and GC-MS (GC-MS values shown in parentheses); [c)]The conversion of DBT and selectivity of products was calculated using GC-MS of fuel phase and ^{1}H NMR spectroscopy of solvent extraction phase and a solvent washing of post-reaction solid catalysts; [d)]Turnover frequency calculated from the conversion of 4% weight loaded MoO_x nanomaterials with 120 min ODS experiment (the value in parenthesis describes the value determined using the conversion obtained after only 30 min).

Interestingly, initial attempts to reuse the MoO_2@GNF catalyst were only moderately successful, with an ≈40% drop in sulfur removal capacity noted after the first cycle (red bars, Figure 6b). Analysis of MoO_2@GNF after the first ODS reaction by PXRD (Figure 6c) revealed the presence of a mixture of organic molecules held within GNFs, comprising predominantly $DBTO_2$, a small amount of DBTO, but importantly no DBT. Complementary TGA (Figure 6d) of the used MoO_2@GNF catalyst confirmed the presence of $DBTO_2$ inside GNFs, with a significant mass loss at 242 °C consistent with the boiling point of the sulfone product (Figure S7, Supporting Information) noted. Moreover, ^{1}H NMR spectroscopy analysis of the organic material removed from the internal channel of GNFs by subsequent washing of the solid catalyst (Figure S8, Supporting Information) confirmed that only DBTO and $DBTO_2$ become adsorbed and trapped within the GNFs in significant quantities. Whilst our adsorption experiments (Table S2, Supporting Information) indicate that MoO_2@GNF only uptakes negligible quantities of DBT from solution by ADS, analysis of the catalyst after its first use provides compelling evidence that enhanced removal of sulfur contaminants can be achieved here by selective adsorption and retention of the products of ODS reaction, i.e., adsorptive desulfurization by sequestration of DBTO sulfoxide and $DBTO_2$ sulfone. This is consistent with a previous study which indicated that the adsorption affinity of porous carbons was significantly greater for $DBTO_2$ than DBT.[41] From a practical point of view, accumulation of the ODS products necessitates an additional thermal or solvent treatment between uses of catalytic nanoreactors MoO_2@GNF in order to maintain the high sulfur removal capacity use-to-use (green bars, Figure 6b). However, this nanosponge effect ensures efficient removal of the sulfur contaminants through a combination of ODS and ADS, thus potentially negating the requirement for a separate and costly additional extraction step (**Figure 7**a).

In light of this, we next considered the efficiency of sulfur contaminant removal in the absence of a solvent extraction step, with over 90% removal of the DBT observed (Table 1, entry 3). Kinetic analysis indicates a pseudolinear removal of DBT up to 60 min, yielding 78% total sulfur removal; after this, the rate of removal decreases from a combination of the expected decrease in DBT concentration as the reaction proceeds and slower diffusion inside the GNF internal channel due to accumulation of the products of DBT oxidation inside nanoreactors (Figure 7b). However, after 60 min the level of sulfur contaminants within the fuel approaches that which is required to meet current ULSD regulations. Similarly, the decrease in activity of MoO_3@GNF (Table 1, entry 4) is a consequence of the confined catalysts growing to the diameter of the nanofiber resulting in blocking of the internal cavity and subsequently restricting access of reactants to the confined catalyst. Given the low catalyst loading in our experiments, our catalytic nanoreactors MoO_2@GNF significantly outperform other catalysts in their ability to desulfurize fuel by more than an order of magnitude (Table S3, Supporting Information).[21,39,42,43]

To assess the effectiveness of the MoO_2@GNF catalysts toward real fuel systems a more sterically demanding contaminant (dimethyl dibenzothiophene – DMDBT) and an electron-poor contaminant (benzothiophene – BT) were investigated alongside DBT in *n*-octane as a more representative fuel. No effect of solvent, i.e., *n*-hexane versus *n*-octane, was noted in the sole oxidation of DBT (Table S4, Supporting Information). From a comparison of the sulfur removal efficiency of GNFs and MoO_2@GNF (including and without the solvent extraction) after 18 h, it is clear that MoO_2@GNF is effective towards the oxidation of organosulfur species, with the nanosponge able to remove the oxidized contaminants from the mixed fuel system (**Table 2**), with the order of reactivity of these contaminants shown to be DMDBT > DBT > BT. After 2 h, it was found that there was almost 100% removal of DMDBT. The reason for this is thought to be related to the higher affinity of DMDBT for GNFs which encourages absorption into the internal channel of the nanoreactors and leads to a high concentration of DMDBT

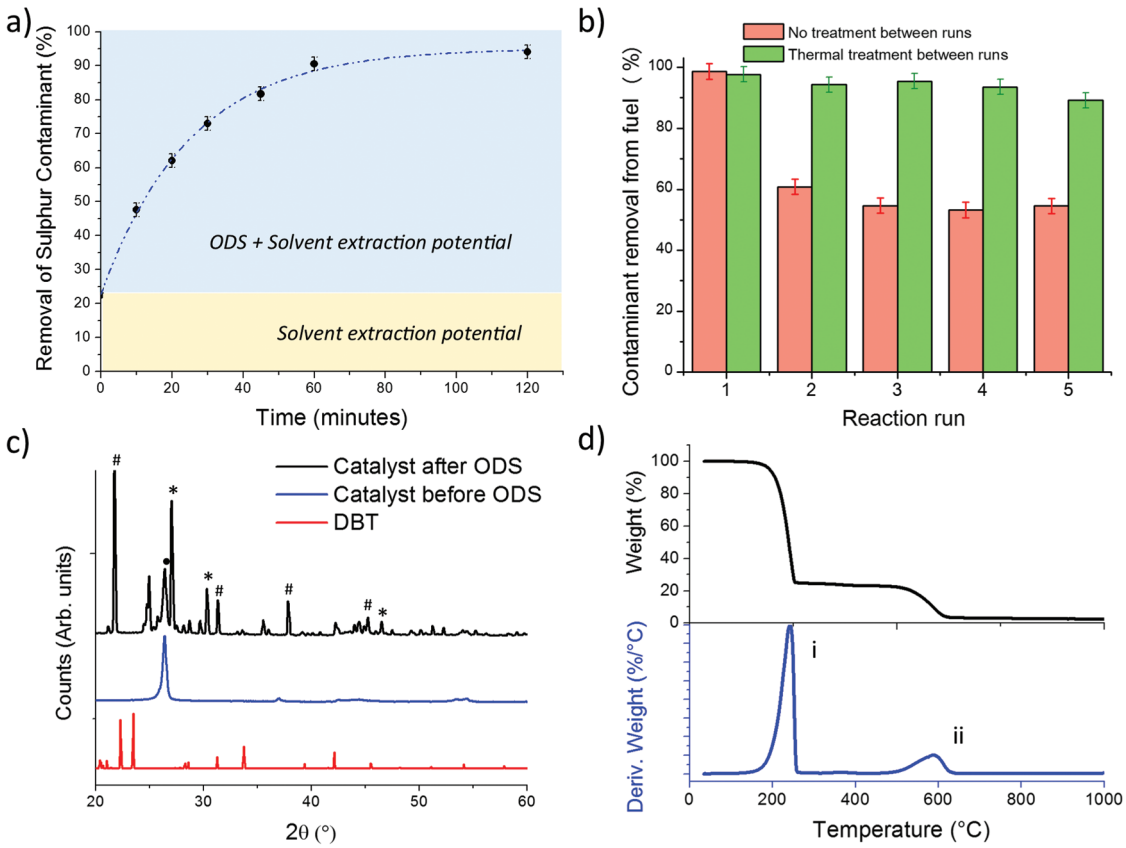

Figure 6. a) Kinetic profile for the removal of DBT from *n*-hexane using the ODS (5 mg MoO_2@GNF, 5 mL fuel, 1:20 S:O ratio, 60 °C, 120 min) and solvent extraction (5:1 hexane:acetonitrile, 30 min) procedures. These results show that there is moderate sulfur removal from the model fuel using solvent extraction alone; however, when combined with the ODS reaction, near complete removal can be achieved on a relatively short timescale. b) Recycling experiments using MoO_2@GNF with no catalyst treatment between runs for the ODS of DBT indicated an ≈40% lower sulfur removal capacity after the first use, with no significant changes noted over the next four uses. Analysis of the used catalyst by PXRD c) indicated the selective retention of the products of ODS (* sulfoxide, # sulfone, • catalyst) within the nanoreactor cavity after the initial use. This was confirmed by d) TGA, with a mass loss at 242 °C (i) consistent with the boiling point of $DBTO_2$, prior to GNF combustion at 589 °C (ii). The presence of the products of ODS within GNFs after the first use provides strong evidence for the ability of MoO_2@GNF to decontaminate model fuels using a dual functional approach, i.e., involving both ODS of DBT and ADS of the ODS reaction products. Moreover, the retention of activity use-to-use after the initial drop, in the absence of an intermediate catalyst washing step, indicates that the products of the ODS reactions do not permanently block the GNF nanoreactor cavity and therefore access of DBT molecules to the catalyst in subsequent uses is not restricted. Thus, the observed reduction in sulfur removal after the initial use reflects the slower accumulation of DBT molecules at the GNF step-edges, requiring initial desorption of the ODS products from the cavity of the used MoO_2@GNF catalyst into the fresh model fuel, i.e., down a $DBTO_2$ concentration gradient, to provide a route for access of new DBT reactant molecules to the catalytic centers. The introduction of either a 250 °C thermal treatment or washing with a polar solvent between consecutive ODS reactions effectively removes these products from the channel and is essential for ensuring high catalytic activity even after five uses (b). A very small drop in catalyst performance is still noted between uses one to five and this has been attributed to subtle changes in nanoparticle morphology and loading induced during successive reactions.

at the location of the catalyst. This is supported by the observation of a small decrease in the removal of DBT in the mixed system from what would be expected after 2 h in isolation, indicative of competition within the nanoreactor of DMDBT and DBT for access to the catalyst (Table 2 – values in parentheses). After an 18 h ODS procedure, all of the DMDBT and DBT can be effectively oxidized and removed by the solid nanosponge extraction process (Table S5, Supporting Information). Although BT can be oxidized by the catalyst, the rate of oxidation is lower than the other contaminants, requiring 18 h for the near total (95%) removal. In all these reactions MoO_2@GNF not only promotes the ODS reactions but also absorbs the products of oxidation via the ADS mechanism leading to desulfurization at ULSD regulations.

3. Conclusion

In this study, we demonstrate that catalytic nanoreactors employed in the desulfurization of liquid fuels play a dual role of catalyst and nanosponge – simultaneously promoting the reactions of oxidation of organosulfur species and absorbing their products from a model fuel. Several group VI metal oxide nanoparticles were grown inside GNF hollow carbon nanofibers

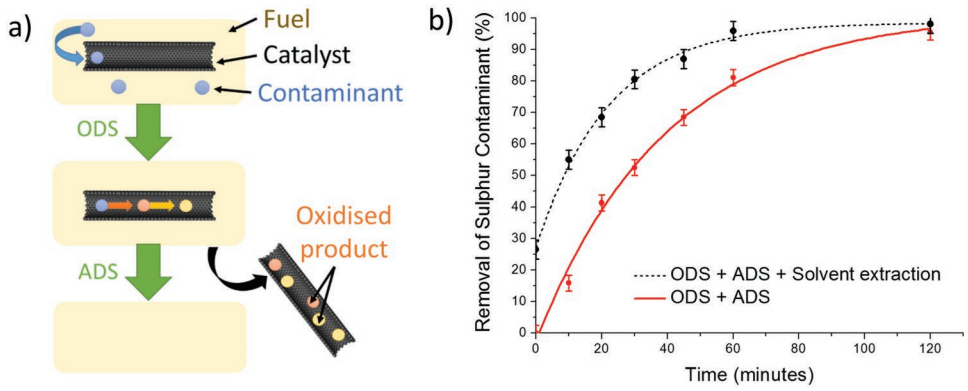

Figure 7. a) Schematic diagram describing the process of oxidation and extraction using the nanoreactor and nanosponge composite material to achieve effective removal of sulfur contaminants. b) Kinetic profile for the removal of DBT from an *n*-hexane model fuel using the ODS procedure alone (5 mg MoO_2@GNF, 5 mL fuel, 1:20 S:O ratio, 60 °C), thus exploiting the nanosponge potential for extraction. These results show that there is a near linear removal of DBT up to 60 min. After 120 min, near complete removal can be achieved without the need for a separate solvent extraction.

and were found to form stable materials with well-defined and controlled structure and composition. Molybdenum (IV) oxide nanoparticles within GNFs (MoO_2@GNF) showed the best catalytic activity resulting in over 98% desulfurization by utilizing the nanosponge's abilities to selectively absorb the oxidized products. ULSD levels of mixed and individual organosulfur contaminated model fuels can be achieved by applying the nanosponge or combined solvent extraction procedure. Confinement of catalytic centers in GNFs allows effective reuse of the nanoreactors for at least 5 cycles with no significant loss of activity. Importantly, the dual ODS and ADS functionality of MoO_2@GNF material negates the need for the extraction stage, leading directly to the removal of over 95% of organosulfur contaminants from the liquid alkane fuels.

4. Experimental Section

General: Standard reagents, including 4,6-dimethyldibenzothiophene (97%), benzothiophene (98%), and thiophene (>99%), and solvents were purchased from Sigma-Aldrich Chemicals and were used as purchased. Additional reagents were obtained from the following sources: dibenzothiophene (98%, Acros Chemicals), *n*-octane (95%, VWR Chemicals), *n*-hexane (98.5%, Fischer Scientific), tert-butyl hydroperoxide (70% aqueous solution, Alfa Aesar), and bis(acetylacetonato)

Table 2. Sulfur removal from a mixed contaminant model fuel system.

Contaminant	GNF[a]		MoO_2@GNF[a]	
	Sulfur removal with ODS procedure[b] [%]	Sulfur removal with ODS and solvent extraction procedures[b] [%]	Sulfur removal with ODS procedure[b] [%]	Sulfur removal with ODS and solvent extraction procedures[b] [%]
BT 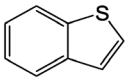	1.6	30.8	94.8 (2.6)	98.3 (44.7)
DBT 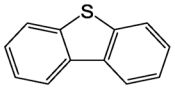	4.1	26.3	100.0 (84.3)	100.0 (94.3)
DMDBT 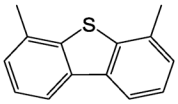	10.9	16.9	100.0 (99.3)	100.0 (99.4)
Sulfur contaminants remaining in fuel[c] [ppm]	354.2	282.5	6.5* (142.2)	2.1* (58.9)

[a]5 mg of heterogeneous catalyst (empty GNF or MoO_2@GNF containing 4 wt% MoO_x), 5 mL of *n*-octane containing three contaminants (125 ppm of benzothiophene – BT, dibenzothiophene – DBT, and dimethyldibenzothiophene – DMDBT), sulfur:oxidant molar ratio is 1:20, tert-butyl hydroperoxide oxidant, 60 °C, 18 h (values in parentheses correspond to data collected after 2 h); [b]Percentage of sulfur-containing contaminants removed via either (i) ODS or (ii) combined ODS and solvent extraction (1 mL CD_3CN, 30 min) was determined using GC-MS; [c]Sum of contaminants removed from the fuel in ppm. * Represent values below those required by current regulations.

dioxymolybdenum(VI) ($MoO_2(CH_3COCHCOCH_3)_2$ (99%, Alfa Aesar). Graphitized nanofibers (PR19-XT-HHT carbon nanofibers, iron content < 100 ppm) were purchased from Pyrograf Products Inc.

Transmission electron microscopy and dark field scanning transmission electron microscopy were performed using a JOEL JEM-2100Plus microscope operated at 200 KeV. TEM samples were prepared via a drop casting technique, where samples were first dispersed in methanol and deposited on a copper grid mounted "lacey" carbon films. All images were processed using Gatan Digital Micrograph. Energy dispersive X-ray spectroscopy and mapping were acquired for samples mounted on the TEM grid using an Oxford Instruments INCA X-ray microanalysis system. The beam was condensed onto areas suspended over holes of the amorphous carbon film to eliminate contributions from the support film itself. The copper and the silicon peak signals, associated with the grid mesh and an artefact of grid fabrication, were removed.

Thermogravimetric analysis was performed using a TA Q500 Thermogravimetric Analyzer. All samples were analyzed using a platinum pan and in the presence of air. The parameters for all experiments were: Ramp 5 °C min^{-1} from 20 to 1000 °C with an isotherm for 10 min at 1000 °C, air flow: 60 mL min^{-1}.

The powder X-ray measurements were performed using a PANalytical X'Pert Pro diffractometer equipped with a Cu K(α) radiation source (λ = 1.5432, 40 kV 40 mA) in Bragg-Brentano geometry using a Si zero background holder. All samples were wetted with isopropyl alcohol to aid GNF adhesion. The parameters for a typical experiment were: start angle: 5°, stop angle: 80°, step size: 0.0525°, time/step: 6080 s, and scan speed: 0.00220° s^{-1}. High temperature PXRD measurements were performed using an Anton Parr (HTK 1200N) high temperature oven chamber in air up to 450 °C.

UV-vis absorption spectra were recorded at room temperature using 1 cm quartz cuvettes. The samples were run using a Perkin-Elmer Lambda 25 UV-vis spectrometer at a scan rate of 240 nm min^{-1} over a wavelength range of 200–500 nm. Spectra were analyzed using UV WinLab ES software. For all analysis, 30 µL of the treated model fuel was diluted using 2.5 mL of the same solvent.

^1H NMR spectroscopy spectra were recorded in CD_3CN at room temperature using a Bruker AVANCE DPX-300 spectrometer (TopSpin 1.3 PL4) in Wilmad NMR tubes (5 mm diameter). Spectra were analyzed using MestReNova software.

Samples were analyzed by GC-MS using a Thermo Scientific ISQ-LT single quadrupole mass spectrometer, attached to a Thermo Scientific Trace 1300 GC. Samples were injected through a Thermo Scientific TriPlusRSH liquid autosampler onto a Thermo Scientific TG5MS GC column (15 m × 0.25 mm × 0.25 µm). Instrument conditions were as follows: GC injector temperature 200 °C; injections were performed in split mode, employing a 50:1 split ratio. The GC oven temperature programme was 40 °C (3 min) to 320 °C (10 min) at 5 °C min^{-1}. The GC carrier gas was helium, with a column flow of 1 mL min^{-1}. The mass spectrometer was programmed to acquire data after a 3 min delay, over the mass range of 50–600 Da, with a 0.2 s scan time. Mass spectra were acquired in EI mode (70 eV ionization energy). The ion source temperature was 200 °C and the MS transfer line was maintained at 250 °C. Total ion current chromatograms and associated mass spectra were processed with Chromeleon software (Version 7.2; Thermo Fisher Scientific Inc., Massachusetts, USA).

Preparation of MO_x@GNF: The molybdenum dioxide catalyst was synthesized by first pretreating PR19 graphitized nanofibers, to remove any moisture, by heating below their oxidation temperature (500 °C) in air for 1 h. The pretreated graphitized nanofibers (60 mg) were then loaded into a Pyrex glass tube (d = 10 mm, L = 6 cm) with molybdenum dioxide bisacetylacetonate (11.1 mg) and sealed under vacuum (≈5×10^{-5} mbar). The sealed vessel was then heated to 160 °C for 2 days. Following sublimation and prior to opening, the Pyrex glass tube was immediately cooled for 5 min. $MoO_2(acac)_2$@GNF were placed into a new Pyrex glass tube (d = 10 mm, L = 6 cm) and evacuated and backfilled with argon (repeated three times) to remove any oxygen or moisture present. Before sealing, the Pyrex glass tube was filled with argon gas (≈0.5 bar). For the decomposition step, the sealed vessels were heated at 500 °C for 1 h in a preheated furnace to obtain the MoO_2@GNF composite material, which was then cooled down slowly for 9 h. MoO_2@graphite composite was synthesized using the same method with a graphite flakes powder to $MoO_2(acac)_2$ ratio of 5.6 mg: 30 mg. For the tungsten/chromium oxide encapsulated species the same procedure was followed with a tungsten hexacarbonyl precursor (6.8 mg, sublimation temperature; 120 °C) or chromium acetylacetonate precursor (25.0 mg, sublimation temperature; 160 °C). Postsynthesis thermal manipulation of the MoO_2@GNF composite required heating at 350 °C in air for 30 min and cooled slowly over 2 h to form MoO_3@GNF.

Oxidative Desulfurization Procedure: The first model fuel (500 mg L^{-1} of sulfur) was prepared by dissolving DBT (0.870 g, 4.72 mmol) in 300 mL *n*-hexane. The second mixed component model fuel contains benzothiophene (125 ppm), dibenzothiophene (125 ppm), and dimethyl dibenzothiophene (125 ppm) in *n*-octane. The desulfurization experiments were conducted at 60 °C. In general, 5 mg of catalyst was added to 5 mL of the model fuel and sonicated for 2 min. 0.14 mL of 70 wt% tert-butyl hydroperoxide (TBHP) aqueous solution was added and the solution was heated for 120 min unless otherwise stated and stirred at 500 rpm. Once complete, the solid was removed and the reaction products extracted using 1 mL CH_3CN. The extraction process was vigorously stirred at a constant speed (1000 rpm) for 30 min at ambient temperature. The removed catalyst was washed with deuterated solvent and the washings were combined with the extraction layer. For the recycling experiments where no catalyst washing was performed between subsequent uses (red bars, Figure 6b) the solid catalyst was separated from the reaction mixture by filtration, without an extraction into acetonitrile, and dispersed directly as a solid in the model fuel of successive reactions. The extraction phase and organic fuel layer were separated and separately analyzed: the *n*-hexane layer by GC-MS, UV–vis and ^1H NMR spectroscopies; the extraction layer using GC-MS and ^1H NMR spectroscopy. The oxidation of DBT was monitored by the disappearance of the characteristic chemical shifts between 8.28 and 8.21 ppm (m, 2H). Confirmation of the sulfoxide and sulfone products was afforded by monitoring by the integrals between 7.71–7.64 (t, 2H) and 7.86–7.81 (d, 2H), respectively. The treated diesel was stored in a sealed vial and kept refrigerated at 2 °C. GC-MS retention times for organosulfur compounds were: DBT = 25.27, DBTO = 32.23, $DBTO_2$ = 32.51; DMDBT = 29.27, DMDBTO = 34.67, $DMDBTO_2$ = 34.48; BT = 11.94, BTO = 21.54, BTO_2 = 22.18 min.

The desulfurization experiments without the solvent extraction were conducted as previously mentioned at 60 °C. In general, 5 mg of catalyst was added to 5 mL of the model fuel and sonicated for 2 min. 0.14 mL of 70 wt% TBHP aqueous solution was added and the solution was heated for 120 min unless otherwise stated and stirred at 500 rpm. Once complete, the solid was removed, with resultant organic phase and washed solid catalyst analyzed using the techniques stated above.

Supporting Information

Supporting Information is available from the Wiley Online Library or from the author.

Acknowledgements

The authors would like to thank the Centre for Sustainable Chemistry (CSC), University of Nottingham, and the Engineering and Physical Science Research Council (EPSRC) for supporting this research, and the Nanoscale and Microscale Research Centre (nmRC) for access to the electron microscopy facilities.

Conflict of Interest

The authors declare no conflict of interest.

Keywords

carbon nanotubes, molybdenum dioxide, nanoreactors, nanosponges, oxidative desulfurization

Received: November 14, 2018
Revised: February 1, 2019
Published online:

[1] S. Mohankumar, P. Senthilkumar, *Renewable Sustainable Energy Rev.* **2017**, *80*, 1227.
[2] A. K. Agarwal, *Prog. Energy Combust. Sci.* **2007**, *33*, 233.
[3] G. Mohebali, A. S. Ball, *Int. Biodeterior. Biodegrad.* **2016**, *110*, 163.
[4] V. C. Srivastava, *RSC Adv.* **2012**, *2*, 759.
[5] H. A. El Sayed, A. M. A. El Naggar, B. H. Heakal, N. E. Ahmed, S. Said, A. A. H. Abdel-Rahman, *Fuel* **2017**, *209*, 127.
[6] E. Ito, J. A. R. van Veen, *Catal. Today* **2006**, *116*, 446.
[7] P. S. Kulkarni, C. A. M. Afonso, *Green Chem.* **2010**, *12*, 1139.
[8] J. Bu, G. Loh, C. G. Gwie, S. Dewiyanti, M. Tasrif, A. Borgna, *Chem. Eng. J.* **2011**, *166*, 207.
[9] M. Armaghan, M. M. Amini, H. R. Khavasi, W. H. Zhang, S. W. Ng, *RSC Adv.* **2016**, *6*, 85381.
[10] L. H. Zhang, J. Y. Wang, Y. L. Sun, B. Jiang, H. W. Yang, *Chem. Eng. J.* **2017**, *328*, 445.
[11] J. Wang, R. R. Butler, F. Wu, J. F. Pombert, J. J. Kilbane, B. C. Stark, *PLoS One* **2017**, *12*, 20.
[12] M. F. Ali, A. Al-Malki, B. El-Ali, G. Martinie, M. N. Siddiqui, *Fuel* **2006**, *85*, 1354.
[13] R. T. Yang, A. J. Hernandez-Maldonado, F. H. Yang, *Science* **2003**, *301*, 79.
[14] A. R. Lopes, A. D. Scheer, G. V. Silva, C. I. Yamamoto, *Materia* **2016**, *21*, 407.
[15] E. Deliyanni, M. Seredych, T. J. Bandosz, *Langmuir* **2009**, *25*, 9302.
[16] D. H. Wang, E. W. H. Qian, H. Amano, K. Okata, A. Ishihara, T. Kabe, *Appl. Catal., A* **2003**, *253*, 91.
[17] M. A. Safa, X. L. Ma, *Fuel* **2016**, *171*, 238.
[18] L. Qiu, Y. Cheng, C. P. Yang, G. M. Zeng, Z. Y. Long, S. N. Wei, K. Zhao, L. Luo, *RSC Adv.* **2016**, *6*, 17036.
[19] J. L. Garcia-Gutierrez, G. A. Fuentes, M. E. Hernandez-Teran, P. Garcia, F. Murrieta-Guevara, F. Jimenez-Cruz, *Appl. Catal., A* **2008**, *334*, 366.
[20] A. Bazyari, A. A. Khodadadi, A. H. Mamaghani, J. Beheshtian, L. T. Thompson, Y. Mortazavi, *Appl. Catal., B* **2016**, *180*, 65.
[21] W. A. W. Abu Bakar, R. Ali, A. A. A. Kadir, W. Mokhtar, *Fuel Process. Technol.* **2012**, *101*, 78.
[22] M. Zhang, W. S. Zhu, S. H. Xun, J. Xiong, W. J. Ding, M. Li, Q. Wang, H. M. Li, *Chem. Eng. Technol.* **2015**, *38*, 117.
[23] Y. Q. Xu, W. M. Xuan, M. M. Zhang, H. N. Miras, Y. F. Song, *Dalton Trans.* **2016**, *45*, 19511.
[24] A. La Torre, M. W. Fay, G. A. Rance, M. Del Carmen Gimenez-Lopez, W. A. Solomonsz, P. D. Brown, A. N. Khlobystov, *Small* **2012**, *8*, 1222.
[25] X. L. Pan, X. H. Bao, *Acc. Chem. Res.* **2011**, *44*, 553.
[26] T. H. Noh, O. S. Jung, *Acc. Chem. Res.* **2016**, *49*, 1835.
[27] W. A. Solomonsz, G. A. Rance, B. J. Harris, A. N. Khlobystov, *Nanoscale* **2013**, *5*, 12200.
[28] A. La Torre, M. D. Gimenez-Lopez, M. W. Fay, G. A. Rance, W. A. Solomonsz, T. W. Chamberlain, P. D. Brown, A. N. Khlobystov, *ACS Nano* **2012**, *6*, 2000.
[29] A. N. Khlobystov, *ACS Nano* **2011**, *5*, 9306.
[30] S. Gupta, N. H. Tai, *J. Mater. Chem. A* **2016**, *4*, 1550.
[31] T. A. Saleh, S. A. Al-Hammadi, A. Tanimu, K. Alhooshani, *J. Colloid Interface Sci.* **2018**, *513*, 779.
[32] T. A. Saleh, *J. Cleaner Prod.* **2018**, *172*, 2123.
[33] J. A. Arcibar-Orozco, J. R. Range-Mendez, T. J. Bandosz, *Energy Fuels* **2013**, *27*, 5380.
[34] M. A. Astle, G. A. Rance, M. W. Fay, S. Notman, M. R. Sambrook, A. N. Khlobystov, *J. Mater. Chem. A* **2018**, *6*, 20444.
[35] P. X. Han, W. Ma, S. P. Pang, Q. S. Kong, J. H. Yao, C. F. Bi, G. L. Cui, *J. Mater. Chem. A* **2013**, *1*, 5949.
[36] R. Y. Zhuang, S. S. Yao, M. X. Jing, X. Q. Shen, J. Xiang, T. B. Li, K. S. Xiao, S. B. Qin, *Beilstein J. Nanotechnol.* **2018**, *9*, 262.
[37] L. P. Hou, R. X. Zhao, X. P. Li, X. H. Gao, *Appl. Surf. Sci.* **2018**, *434*, 1200.
[38] A. Alizadeh, M. Fakhari, M. M. Khodeai, G. Abdi, J. Amirian, *RSC Adv.* **2017**, *7*, 34972.
[39] M. Chamack, A. R. Mahjoub, H. Aghayan, *Chem. Eng. J.* **2014**, *255*, 686.
[40] I. Martinez, M. E. S. Mohamed, D. Rozas, J. L. Garcia, E. Diaz, *Metab. Eng.* **2016**, *35*, 46.
[41] Y. W. Shi, G. Z. Liu, X. W. Zhang, *Ind. Eng. Chem. Res.* **2017**, *56*, 2557.
[42] H. Y. Ji, H. T. Ju, R. Lan, P. W. Wu, J. Sun, Y. H. Chao, S. H. Xun, W. S. Zhu, H. M. Li, *RSC Adv.* **2017**, *7*, 54266.
[43] M. Chamack, A. R. Mahjoub, *Catal. Lett.* **2016**, *146*, 1050.